Modeling Dam Break Behavior over a Wet Bed by a SPH Technique

A. J. C. Crespo[1]; M. Gómez-Gesteira[2]; and R. A. Dalrymple, F.ASCE[3]

Abstract: Dam break evolution over dry and wet beds is analyzed with a smoothed particle hydrodynamics model. The model is shown to accurately fit both experimental dam break profiles and the measured velocities. In addition, the model allows one to study different propagation regimes during the dam break evolution. In particular, different dissipation mechanisms were identified: bottom friction and wave breaking. Although breaking dominates over wet beds at the beginning of the movement, bottom friction becomes the main dissipation mechanism in the long run.

DOI: 10.1061/(ASCE)0733-950X(2008)134:6(313)

CE Database subject headings: Numerical models; Fluid flow; Dam failure; Laboratory tests; Water waves.

Introduction

Typical dam break experiments show a rapidly moving tongue of water generated by the instantaneous release of a given volume of water confined in a rectangular channel. Ritter (1892) introduced a theoretical description of the two-dimensional dam break problem for an inviscid fluid on a dry bed by solving the nonlinear shallow water equations. The solutions provide a parabolic water surface profile that is concave upward. The front travels downstream with a celerity $c=2\sqrt{gd_0}$, where g=acceleration due to gravity, and d_0=initial quiescent water depth behind the dam. Although the theoretical approach assumes no boundary friction, experiments show good agreement with the theory, except for the leading edge of the wave as bottom friction affects the leading tip significantly. Actually, for a horizontal dry channel, the wave front celerity was observed to depend on time. The problem becomes much more complex when the dam break wave propagates over preexisting still water (with an initial depth $d>0$ (Henderson 1966; Montes 1998). In this case, the wave front celerity can be fitted in terms of d and d_0. Leal et al. (2006) examine the influence of erodible beds. In spite of previous studies, the dynamics of dam breaks are far from being completely understood, especially when the wave front advances over a wet bed. Apart from the theoretical interest of this configuration, it can also contribute to the understanding of tsunamigenic waves when reaching the shoreline as mentioned in Chanson et al. (2003).

Models based on smoothed particle hydrodynamics (SPH) are an option to address dam break evolution. SPH is a Lagrangian method developed during the 1970s (Lucy 1977; Gingold and Monaghan 1977) in astrophysics, which can be easily applied to other fields due to its conceptual simplicity. Thus, the method has been used to simulate impacts in solids (Benz and Asphaug 1994, 1995) and free surface hydrodynamics problems (Monaghan 1996; Monaghan et al. 1999; Monaghan 1994; Monaghan and Kos 1999, 2000). In particular, the method has shown to be well suited to analyze wave impact on offshore structures (Dalrymple et al. 2002; Gómez-Gesteira and Dalrymple 2004; Gómez-Gesteira et al. 2005, Crespo et al. 2007b). The Lagrangian nature of SPH provides the method with some advantages when compared to the usual limitations in Eulerian methods. On the one hand, the density number of particles increases in regions where the fluid is present, in such a way that the computational effort is mainly concentrated in those regions. On the other hand, there are no constraints imposed either on the geometry of the system or in how far it may evolve from the initial conditions, such that the initial conditions can be easily programmed without the need of complicated gridding algorithms as used in finite-element methods.

However, the method also presents some intrinsic limitations. For example, boundary condition implementation is a hard task and fluid particles penetration into boundaries must be avoided. In addition, the interpolation method used in SPH is very simple and it will be strongly affected by particle disorder. SPH gives reasonable results for the first-order gradients [although Bonet and Lok (1999) recommend gradient corrections], but they can be worse for higher order derivatives. Sometimes it is necessary to use special techniques when second derivatives are included. Finally, the method is typically slower computationally when compared to other modern grid-based methods, as the time step is based on a sound speed in the fluid—although new research has been developed during the last few years to overcome these limitations.

A dam break over a dry bed has been previously treated using SPH techniques (Monaghan 1994; Colagrossi and Landrini 2003; Gómez-Gesteira and Dalrymple 2004; Violeau and Issa 2006; Crespo et al. 2007a) showing reasonable accuracy with experiments. However, as far as we know, the method has only been

[1]Graduate Student, Grupo de Física de la Atmósfera y del Océano, Facultad de Ciencias, Univ. de Vigo, 32004 Ourense, Spain. E-mail: alexbexe@uvigo.es

[2]Professor Titular, Grupo de Física de la Atmósfera y del Océano, Facultad de Ciencias, Univ. de Vigo, 32004 Ourense, Spain. E-mail: mggesteira@uvigo.es

[3]Hackerman Professor, Dept. of Civil Engineering, Johns Hopkins Univ., 3400 N. Charles St., Baltimore, MD 21218 (corresponding author). E-mail: rad@jhu.edu

Note. Discussion open until April 1, 2009. Separate discussions must be submitted for individual papers. The manuscript for this paper was submitted for review and possible publication on November 14, 2006; approved on April 4, 2008. This paper is part of the ***Journal of Waterway, Port, Coastal, and Ocean Engineering***, Vol. 134, No. 6, November 1, 2008. ©ASCE, ISSN 0733-950X/2008/6-313–320/$25.00.

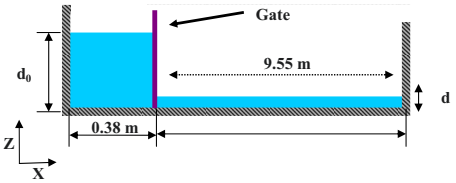

Fig. 1. Schematic arrangement and geometric dimensions of dam-break experiments

previously applied to wet beds in Gómez-Gesteira and Dalrymple (2004), although they considered a very thin water layer close to the bed.

The aim of this paper is the study of the dam break problem and the effect of standing water in front of the dam with the SPH model. The method will be shown to accurately fit the experimental results. In addition, the model captures most of the features of a dam break over a wet bed; in particular, it allows analyzing the mixing and dissipation associated with the interaction between the dam break and the still water placed near the bed.

Experiment

Here we use laboratory experiments by Janosi et al. (2004) to validate a SPH model of dam break evolution over a wet bed. The schematic arrangement of their experimental tank, which has two parts, is shown in Fig. 1. The channel, beginning at $x=38$ cm, is 955 cm long and 15 cm wide. The bottom and side walls of the channel were constructed with glass; the second part, comprising the lock and lock gate, is 38 cm long and made from Plexiglas. The initial fill height of the lock (d_0) for our comparisons is taken as 0.15 m. The initial water depth in the channel downstream of the lock was varied depending on the experiment. The experiments were recorded by two charge-coupled device (CCD) cameras: a fixed fast-shutter camera (Sensicam, PCO Imaging), which provided the side or plan views and another small portable camcorder (Sony DCRPC115E) was fixed on a trolley that was moved along the tank, following the front. The position of the water front as a function of time was determined from digitized pictures. The gate separating the lock from the rest of the tank was removed from above at an approximate constant velocity ($V_{\text{gate}}=1.5$ ms^{-1}).

SPH Methodology

The main features of the SPH method, which is based on integral interpolants, are described in detail in Monaghan (1982, 1992), Benz (1990), and Liu (2003) and we will only refer here to the representation of the constitutive equations in SPH notation. The key idea is to consider that a function $A(\mathbf{r})$ can be interpolated by

$$A(\mathbf{r}) = \int A(\mathbf{r}')W(\mathbf{r}-\mathbf{r}',h)d\mathbf{r}' \tag{1}$$

where h=smoothing length. This approximation, in discrete notation, leads to

$$A(\mathbf{r}) = \sum_b m_b \frac{A_b}{\rho_b} W_{ab} \tag{2}$$

where a and b=particles, m_b and ρ_b=mass and density, respectively, and $W_{ab}=W(r_a-r_b,h)$=weight function or kernel.

Choice of Weight Function

Weight functions, or kernels, determine the intensity of the interaction between adjacent fluid masses (particles). Although the kernel definition is not unique, it mainly depends on the experience of the different researchers (Monaghan 1992; Benz 1990, Liu 2003): all kernels should fulfill the following mathematical constraints: positivity, compact support, normalization, monotonically decreasing, and delta function behavior (in the limit of infinitely small support). The smoothing length h determines the area around particle a where a test particle b has a non-negligible effect on the dynamics of particle a. The cubic spline kernel developed by Monaghan and Lattanzio (1985) was used in our simulations

$$W_{ab} = \frac{1}{\pi h^3}\begin{cases} 1-\frac{3}{2}q^2+\frac{3}{4}q^3 & \text{if } 0 \leqslant q \leqslant 1 \\ \frac{1}{4}(2-q)^3 & \text{if } 1 \leqslant q \leqslant 2 \\ 0 & \text{otherwise} \end{cases} \tag{3}$$

where $q=r/h$; r=distance between particles a and b; and h =smoothing length in SPH and a measure of the compact support. Other kernels such as those described in Liu (2003) can be used with similar results. Due to the particular choice of this kernel, whose first derivative goes to zero with q, the tensile instability correction proposed by Monaghan (2000) was used to prevent particle clumping. In addition, the constant correction proposed by Bonet and Kulasegaram (2000) was used to normalize the kernel. In the following, W_{ab}, will refer to the corrected kernel.

Momentum Equation

Different approaches have been considered in the SPH method to describe the momentum equation due to the different formulations of the diffusive terms.

The artificial viscosity proposed by Monaghan (1992) has been classically used due to its simplicity. In SPH notation, the momentum equation can be written as

$$\frac{d\mathbf{v}_a}{dt} = -\sum_b m_b\left(\frac{P_b}{\rho_b^2}+\frac{P_a}{\rho_a^2}+\prod_{ab}\right)\nabla_a W_{ab} + \mathbf{g} \tag{4}$$

where $\mathbf{g}=(0,0,-9.81)$ ms^{-2}=gravitational acceleration, Π_{ab} =viscosity term

$$\prod_{ab} = \begin{cases} \dfrac{-\alpha\overline{c_{ab}}\mu_{ab}+\beta\mu_{ab}^2}{\overline{\rho_{ab}}} & \mathbf{v}_{ab}\mathbf{r}_{ab} < 0 \\ 0 & \mathbf{v}_{ab}\mathbf{r}_{ab} > 0 \end{cases} \tag{5}$$

with $\mu_{ab}=h\mathbf{v}_{ab}\mathbf{r}_{ab}/\mathbf{r}_{ab}^2+\eta^2$, where $\mathbf{r}_{ab}=\mathbf{r}_a-\mathbf{r}_b$ and $\mathbf{v}_{ab}=\mathbf{v}_a-\mathbf{v}_b$; $\mathbf{r}_k$ and $\underline{\mathbf{v}_k}$=position and the velocity corresponding to particle k (a or b); $c_{ab}=c_a+c_b/2$, $\eta^2=0.01\ h^2$; and α and β=parameters with different values according to each problem. Following Monaghan (1992), β will be considered to be zero.

Continuity Equation

In the SPH method, the fluid is assumed to be weakly compressible, which allows the use of an equation of state to determine

fluid pressure rather than solving another differential equation. However, the compressibility is adjusted to slow the speed of sound so that the time step in the model (based on the speed of sound) is reasonable. Since the speed of sound is not important in this problem, we can slow the speed of sound to be a value no lower than ten times the speed of the dam break tongue, based on Monaghan's (1994) empirical rule of thumb to mimic incompressible fluid behavior.

Changes in the fluid density were calculated by means of

$$\frac{d\rho_a}{dt} = \sum_b m_b \mathbf{v}_{ab} \nabla_a W_{ab} \tag{6}$$

instead of using a weighted summation of mass terms (Monaghan 1992), which leads to an artificial density that decreases near fluid interfaces.

Equation of State

Following Monaghan et al. (1999) and Batchelor (1974), the relationship between pressure and density was assumed to follow the expression

$$P = B\left[\left(\frac{\rho}{\rho_0}\right)^{\gamma} - 1\right] \tag{7}$$

where $\gamma=7$ and $B=c_0^2\rho_0/\gamma$, $\rho_0=1{,}000$ kg m^{-3}=reference density, and $c_0=c(\rho_0)$=speed of sound at the reference density.

XSPH Correction

Particles are moved using the XSPH variant due to Monaghan (1989)

$$\frac{d\mathbf{r}_a}{dt} = \mathbf{v}_a + \varepsilon \sum_b \frac{m_b}{\overline{\rho_{ab}}} \mathbf{v}_{ba} W_{ab} \tag{8}$$

where $\varepsilon=0.5$, and $\overline{\rho_{ab}}=(\rho_a+\rho_b)/2$. This method moves the particle with a velocity that is close to the average velocity in its neighborhood.

SPH Implementation

Initial Conditions: Fluid Particles

Fluid particles were initially placed on a staggered grid with zero initial velocity. Nodes of the grid are located at $R=ldxi+mdzk$ with a two-point basis (0,0) and $(dx/2, dz/2)$ referred to the corner defined by R. l and m=integers, i, k=unitary vectors in X, Z directions, and $dx=dz=0.005$ m. A smoothing length $h=0.006$ m, was considered in all simulations.

The particles are assigned an initial density ρ_0 based on hydrostatic pressure as given by

$$\rho(x,z) = \rho_0\left(1 + \frac{\rho_0 g(H(x)-z)}{B}\right)^{1/\gamma} \tag{9}$$

where $H(x)$=water column height at position x, and z=vertical distance from the bottom.

Boundaries

Due to the particular geometry of the numerical experiment, two different boundary conditions were considered: fixed particles and gate particles. All of them are treated as dynamic boundary particles (Gómez-Gesteira and Dalrymple 2004; Gómez-Gesteira et al. 2005), since they follow the continuity equation and the equation of state, but they do not follow the momentum equation and the XSPH variant, in such a way that their position and velocity are externally fixed. See Crespo et al. (2007a) for a complete description of dynamic boundary particles. Fixed particles (including bottom and fixed walls) are placed in two rows forming a staggered grid with $dx=dz=0.005$ m and zero initial velocity. Their positions and velocities remained unchanged during the numerical experiment.

Gate particles are initially placed in a single row with a finer interparticle spacing $(dx/2, dz/2)$ to prevent particle penetration. Their velocities and positions are externally imposed to mimic the experimental movement of the gate according to $[V_x(t)=0.0$ ms^{-1}; $V_z(t)=1.5$ ms$^{-1}]$. The movement of this gate will play a key role when fitting numerical results to experimental ones, since the gate velocity is on the same order of magnitude as the wavefront celerity $c\cong 2\sqrt{gd_0}\cong 2$ ms^{-1}, in such a way that the experimental and numerical conditions are far from the usual dam break approach, where the gate between the lock and the channel is not considered.

Numerical Parameters

The parameter B in the equation of state (Batchelor 1974) was chosen to guarantee that the speed of sound is a factor of ten larger than the velocities in the model. This can be achieved by taking $B=100gH_{\text{ref}}\rho_0/\gamma$, where H_{ref}=maximum water height in the tank (0.15 m in the numerical experiments). The viscosity term given by Monaghan (1992) was calculated using $\alpha=0.08$ and $\beta=0$. In addition, fluid particles were moved using the so called XSPH (Monaghan 1989) with $\varepsilon=0.5$.

The numerical tank was 9 m long and 0.16 m deep. The number of boundary particles was 3,879. The number of fluid particles depends on the experiment [specifically, the thickness of the water layer (d) in the channel before the gate is lifted]. It ranges from 4,484 for dam break movement on a dry bed to 30,884 with a water layer comparable to the initial dam break height $(d=0.078$ m).

Time Stepping

The Verlet algorithm (Verlet 1967), was used in our numerical simulations. The basic idea of the algorithm is to write two third-order Taylor expansions for the positions, one forward and one backward in time

$$\mathbf{v}_a^{n+1} = \mathbf{v}_a^{n-1} + 2\Delta t \mathbf{F}_a^n$$

$$\mathbf{r}_a^{n+1} = \mathbf{r}_a^n + \Delta t \mathbf{V}_a^n + 0.5\Delta t^2 \mathbf{F}_a^n \tag{10}$$

where $\mathbf{F}_a=(d\mathbf{v}_a)/(dt)$ and $\mathbf{V}_a=d\mathbf{r}_a/dt$.

Time-step control involves the Courant condition, the force terms, and the viscous diffusion term (Monaghan 1989). A variable time step δt was calculated according to (Monaghan and Kos 1999)

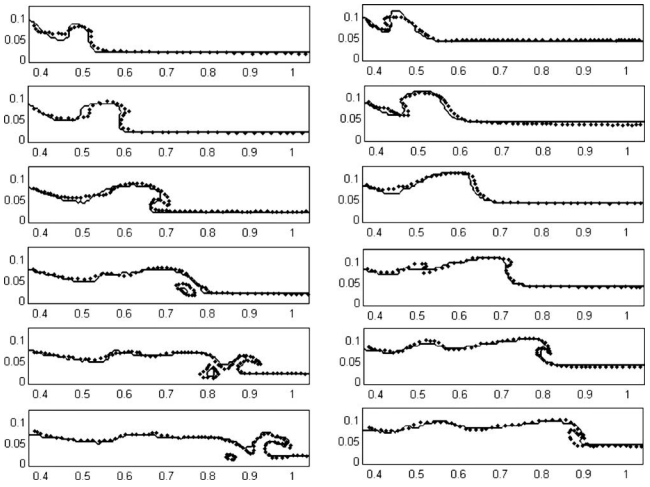

Fig. 2. Comparison between experimental and numerical profiles of dam-break evolution over wet bed, left column (d=0.018 m); right column (d=0.038 m), experimental values are represented by dots and numerical ones by line

$$\delta t = 0.3 \cdot \min(\delta t_f, \delta t_{\text{cv}}) \quad \delta t_f = \min_a \left(\sqrt{\frac{h}{|\mathbf{f}_a|}} \right)$$

$$\delta t_{\text{cv}} = \min_a \frac{h}{c_s + \max_b \left| \frac{h \mathbf{v}_{ab} \mathbf{r}_{ab}}{\mathbf{r}_{ab}^2} \right|} \tag{11}$$

Here δt_f is based on the force per unit mass $\mathbf{f}_a$ [which corresponds to all forces exerted on the particle a following Eq. (4)], and δt_{cv} combines the Courant and the viscous time-step controls. Typically, during the numerical runs, the time step decreases as the water velocity and the force per unit mass increase.

Model Validation

Wave Profiles

Experimental wave profiles (Janosi et al. 2004) were digitized for comparison with SPH results. The dimensions of the digitized snapshots are 0.38 m$\leqslant X \leqslant$1.04 m and 0.0 m$\leqslant Z \leqslant$0.13 m. Distances were measured from the lower left corner of the tank.

Two cases (Fig. 2) with different d values (0.018 and 0.038 m) were considered to compare numerical results and experiments. Experimental values are represented by dots and SPH values by a line. The model is observed to reproduce the experimental profiles in both cases. For d=0.018 m (left column) the water initially placed behind the gate pushes the still water (first and second snapshots), generating the "mushroom" jet mentioned by Janosi et al. (2004) and first reported by Stansby et al. (1998), which suffers successive breakings. Bubble capture is reproduced by the model. A similar accuracy in numerical results is observed for d=0.038 m (right column). Only wave breaking is observed in this case.

Apart from this visual comparison, the observed difference between numerical and experimental results can be quantified considering two statistical parameters, comprised of experimental and numerical values

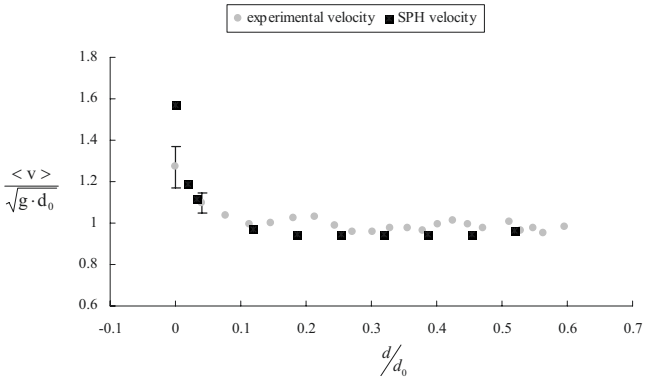

Fig. 3. Comparison between experimental (light circles) and numerical (dark squares) dam-break velocity. Velocity was averaged in space during first 3 m in both cases.

$$A = \sqrt{\sum_{i=1}^{N} (\text{Val}_i^{\text{num}})^2 \Big/ \sum_{i=1}^{N} (\text{Val}_i^{\text{exp}})^2}$$

$$P = \sqrt{\sum_{i=1}^{N} (\text{Val}_i^{\text{num}} - \text{Val}_i^{\text{exp}})^2 \Big/ \sum_{i=1}^{N} (\text{Val}_i^{\text{exp}})^2} \tag{12}$$

A perfect agreement between experiment and numerical model should result in $A \to 1$ and $P \to 0$. The good results obtained for d=0.018 m (left column in Fig. 2: A=1.014, P=0.076) and d=0.038 m (right column in Fig. 2: A=1.012, P=0.058) show the accuracy of the method.

Wave Front Velocity

The experimental and numerical velocities were averaged in space along the first 3 m of the tank (Fig. 3). Numerically, the position of the leading edge was calculated every 0.06 s and velocity was obtained by linear fitting. Both velocities and distances are depicted in a dimensionless form. Velocity is normalized with $c=\sqrt{gd_0}$ and d/d_0 is the ratio between the depth of the fluid layer near the bed and the initial dam height. The normalized velocity is observed to decrease with d. The agreement between experimental measurements (light dots) and numerical results (dark squares) is excellent in most of the cases. Note that SPH velocity for a dry bed is higher than observed in the experiments, since experiments were not performed on a real dry bed, due to the impossibility of completely drying the tank.

Dam-Break Analysis

Now that SPH has been shown to provide accurate results on dam-break propagation, it can be used to analyze the dynamics of that propagation.

Mixing Process

Dam-break propagation on a wet bed is strongly dependent on the interaction between both fluids. From now on, we will refer to the water initially placed behind the gate as *lock water* and to the still water initially placed beyond the gate as *tank water*.

As SPH is a Lagrangian method, the trajectories of all the fluid particles is known. In the Janosi et al. (2004) experiments, clear

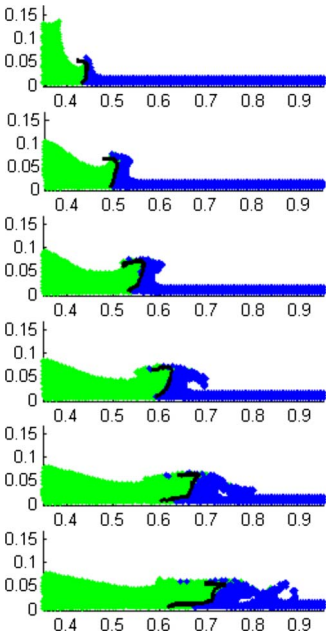

Fig. 4. Experimental and numerical interface between lock and tank water (d=0.015 m); light colors correspond to lock water, dark colors to tank water, and black line to experimental interface

water was released into a channel filled with dyed water. SPH is able to accurately reproduce the interface between both liquids as is shown in Fig. 4 corresponding to d=0.015. The numerical interface between lock water (light color) and tank water (dark color) coincides with the experimental interface (black line) calculated from the Janosi et al. (2004) experiments (see Fig. 14 in their manuscript).

Of course, the model does not pretend to reproduce the dispersion observed near the interface in the experiments. The existence of an area of partially dyed water—light colors in Fig. 14 (Janosi et al. 2004)—comes from the mixing between dyed (dark colors) and clear water (transparent). This mixing cannot be obtained in numerical simulations, where colors represent the origin of particles. Thus, the presence of a few clear particles in the dyed area (or vice versa) is masked by the massive presence of dyed particles in that area.

Fig. 5 represents different instances during the dam-break propagation for different fluid depths (d). The dimensions of the snapshots are 0.0 m$\leqslant X\leqslant$1.6 m and 0.0 m$\leqslant Z\leqslant$1.6 m. The observed behavior depends on the thickness of the water layer near the bed. For d=0.018 m, lock water lifts the tank water near the contact point, which results in successive wave breakings as previously shown in Fig. 2. A similar behavior with only a break was observed for d=0.038 and 0.058 m. Nevertheless, the generation of a wave train was observed for d=0.078 m. In spite of different transient behaviors observed for each configuration, the overall behavior is similar in all cases: lock water mainly pushes tank water without significant mixing. Only for d=0.018 m is there some mixing close to the lock water tip due to the successive breakings as previously shown by Janosi et al. (2004). In addition, the higher the fluid level in the channel d, the smaller the displacement of the lock water (see different columns in Fig. 5) as pointed out by Janosi et al. (2004).

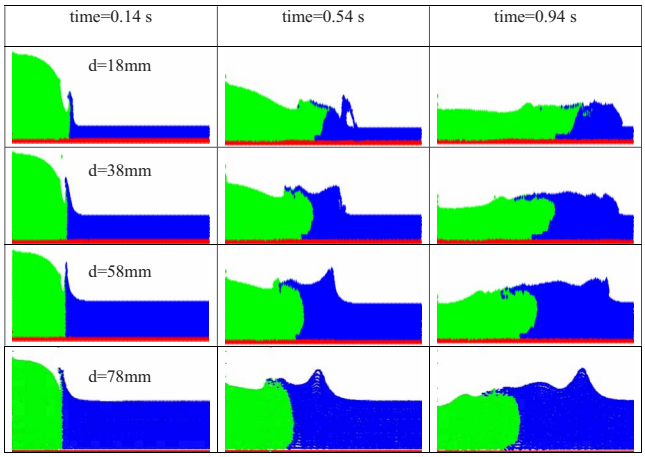

Fig. 5. Different instances of dam evolution for different fluid depths; light colors correspond to lock water and dark colors to tank water

Dam-Break Evolution

The advance of a dam break on a wet bed is far from being a stationary process, especially at the beginning of the movement, where the interaction between both fluids gives rise to different behaviors depending on the depth ratio d/d_0 as previously shown. Thus, different propagation regimes can be observed depending on the zone: the observed horizontal velocity is considerably faster along the first 3 m (dark squares in Fig. 6) than along the first 6 m (light circles in Fig. 6). In addition, the fastest propagation corresponds along the first 3 m to the dry bed and decreases with d. Note that the initial interaction between both fluids results in strong vertical displacements and vorticity generation, which tend to slow down horizontal propagation. The opposite behavior is observed when averaging in space along the first 6 m. The slowest propagation in the X direction corresponds to the dry bed in this case. Movement is mainly controlled by bottom friction during the second 3 m, which is enhanced when reducing the standing water depth.

We should note that the average velocity in space is almost independent of the water level in the channel if $d/d_0>0.1$, this result is consistent with theoretical predictions (Klemp et al. 1997).

Changes in horizontal velocity can be dramatic when lock water starts propagating (along the first 3 m). Thus, the mean

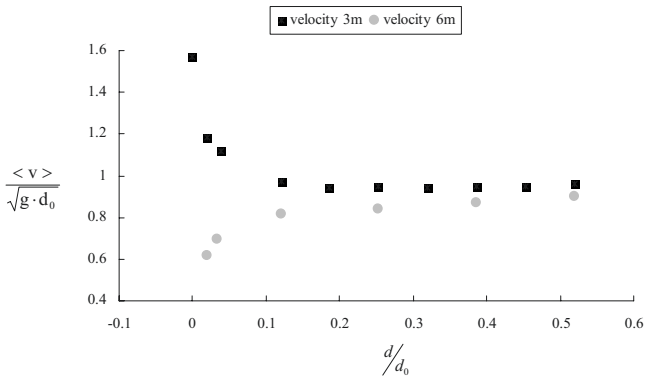

Fig. 6. Spatial average of velocity along first 3 m (dark squares) and first 6 m (light circles) for different fluid depths

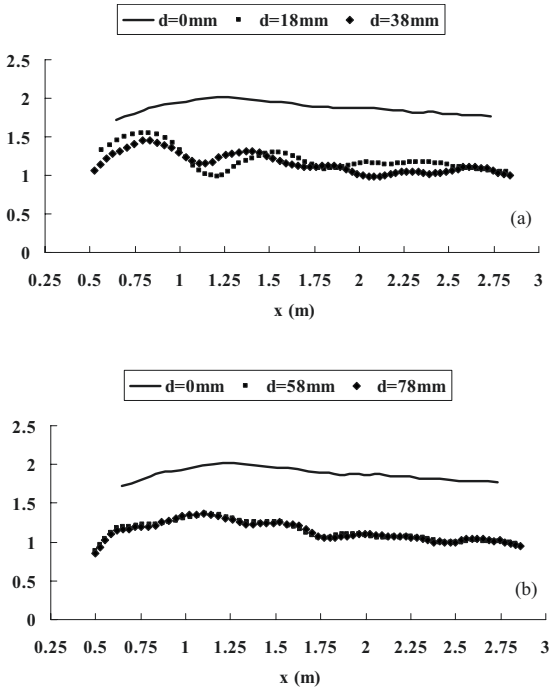

Fig. 7. Velocity evolution with distance for different d values

values shown in Fig. 6 are far from instantaneous velocities, which are strongly dependent on the interaction between both fluids. Fig. 7 shows the instantaneous horizontal velocity measured during the first 3 m. Fig. 7(a) corresponds to a comparison between the dry bed and $d=18$ and 38 mm, and Fig. 7(b) corresponds to a comparison between the dry bed and $d=58$ and 78 mm. First of all, the velocity corresponding to the dry bed (black solid line) is considerably faster than in the rest of the cases. Velocity is observed to increase slightly during the first 1.25 m and decreases from then on. The velocities corresponding to wet beds are considerably slower and present marked oscillations. These oscillations are especially marked for shallow water layers, $d=18$ and 38 mm [Fig. 7(a)], where local minima in velocity correspond to wave breakings shown in Fig. 2. Thus, for example, the strong velocity decrease observed from 0.8 to 1.2 m corresponds to the first wave breaking and eddy generation.

Energy Dissipation

The transition between both propagation regimes can be studied in terms of the dissipated energy. This energy can be defined as

$$\Delta E(t) = \left(\sum_{i=1}^{N} E_i^{\text{kinetic}}(t=0) + \sum_{i=1}^{N} E_i^{\text{potential}}(t=0) \right) - \left(\sum_{i=1}^{N} E_i^{\text{kinetic}}(t) + \sum_{i=1}^{N} E_i^{\text{potential}}(t) \right) \quad (13)$$

where N=number of fluid particles. Note that this definition (in terms of an increment) allows us to compare different experiments, where the amount of fluid and hence the number of fluid particles is different.

Fig. 8 shows the energy dissipated in different experiments over a wet bed ($d=0.018$, 0.038, 0.058, and 0.078 m) and over a dry bed ($d=0$ m). Energy dissipation is observed to increase in time in all cases. In addition, when considering experiments over

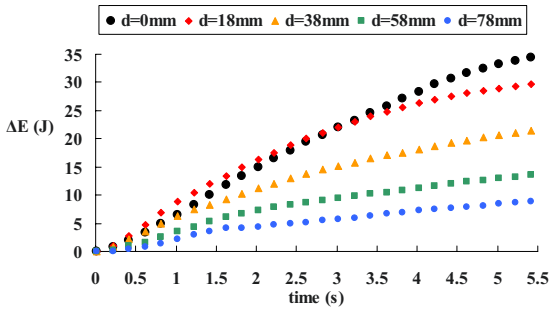

Fig. 8. Energy dissipation for different d values

a wet bed, the energy dissipation measured at each particular instant is observed to be higher for small d values, decreasing monotonically with d. The behavior observed over a dry bed is completely different, where energy dissipation measured at the beginning of the movement is lower than in the rest of the cases since the interaction between both fluids constitutes the dominant dissipation mechanism. However in time, bottom friction becomes the main dissipation mechanism in such a way that energy dissipation becomes higher over a dry bed than over wet beds. Vorticity is analyzed for different fluid depths to better understand this effect.

Vorticity

As SPH is a Lagrangian method, the trajectories of each particle are known every instant and the vorticity of particle a is estimated by Monaghan (1992)

$$\mathbf{w}_a = (\nabla \times \mathbf{v})_a = \sum_b m_b \frac{\mathbf{v}_a - \mathbf{v}_b}{\rho_a} \nabla W_{ab} \quad (14)$$

The next figures (Figs. 9–11) show the Y component of vor-

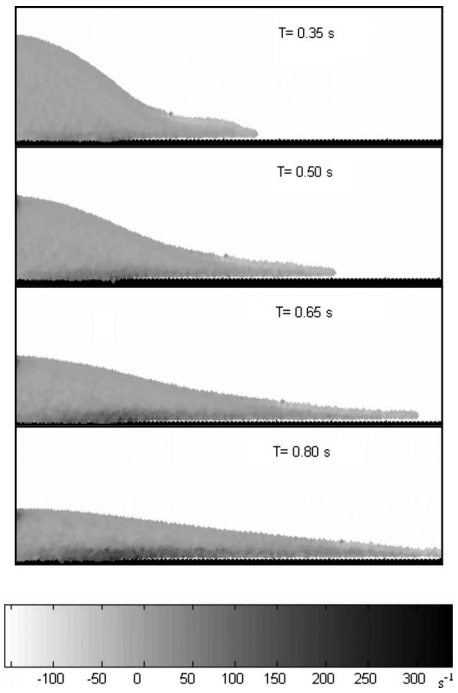

Fig. 9. Vorticity plot for $d=0$ m

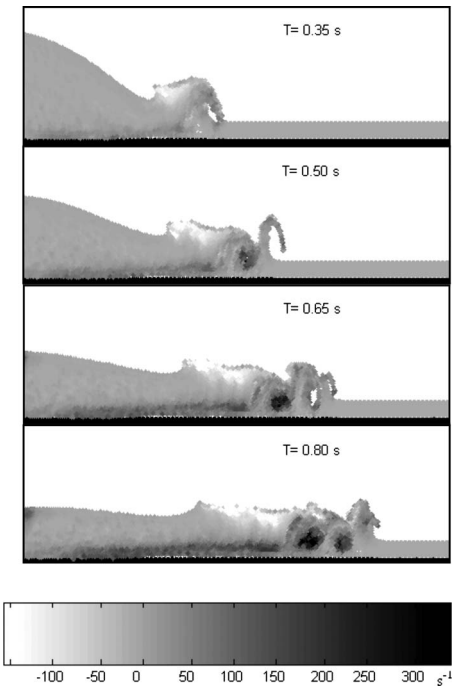

Fig. 10. Vorticity plot for $d=0.018$ m ($d/d_0=0.12$)

ticity (perpendicular to the X and Z planes, see Fig. 1). Positive vorticity values (dark colors) correspond to clockwise rotation and negative ones (light colors) correspond to counterclockwise rotation. The dimensions of the snapshots are $0.0\ \text{m} \leqslant X \leqslant 1.6$ m and $0.0\ \text{m} \leqslant Z \leqslant 0.16$ m.

First, vorticity was calculated in dam-break evolution for a dry bed (Fig. 9). The highest negative values appear in the tip of the dam and positive values appear near the bed due to bottom friction.

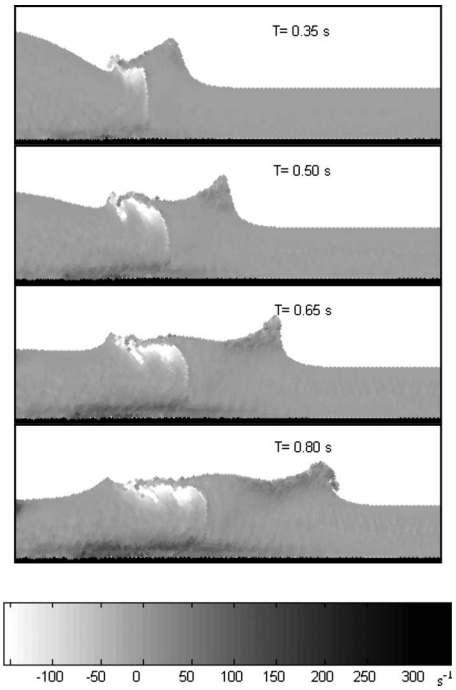

Fig. 11. Vorticity plot for $d=0.058$ m ($d/d_0=0.39$)

Analyzing different instants for $d=0.018$ m (Fig. 10), the wave formation is observed in this case. The water initially placed behind the gate pushes the initially still water (first snapshot), generating the "mushroom" jet mentioned by Janosi et al. (2004). Negative vorticity appears on the left side of this "mushroom" (light colors) due to counterclockwise water rotation. $T=0.35$ s shows first breaking that then generates the first positive eddy (dark colors in $T=0.50$ s). $T=0.65$ s shows the second breaking that is going to generate a second positive eddy (dark colors in $T=0.80$ s).

Vorticity for $d=0.058$ m is also calculated (Fig. 11). Positive values appear mainly near the bed due to close to bottom friction. There is no wave breaking so there are no positive eddies. Water initially placed behind the gate pushes the still water initially placed beyond the gate without significant mixing. The interface of the two water masses is clear and it coincides with the negative vorticity (light colors).

Conclusions

The two-dimensional (2D) version of the SPH model proved to be a suitable tool to reproduce a dam break evolution over dry and wet beds. Experimental profiles and horizontal velocities are properly reproduced by the model.

The mixing process observed in the experiments over a wet bed between lock and tank water is almost negligible. Actually, the basic propagation mechanism is due to the pressure exerted by lock water on tank water. Some mixing is observed in experiments with a shallow water layer, where the successive wave breakings result in eddy generation.

Two regimes are defined in dam evolution. Initial propagation (dam release) in the horizontal direction is faster than observed for longer distances where velocity is mainly reduced by bottom friction. The difference between both regimes is higher for dry beds and shallow water layers.

Energy dissipation was observed to be responsible for both regimes. Energy dissipation for wet beds is higher at the beginning of the experiments, since breaking constitutes the main dissipation mechanism. However in time, bottom friction becomes the main dissipation mechanism, which is especially important for dry beds.

Vorticity is shown to depend on the fluid depth (d). Thus, when the dam break propagates over a dry bed, positive vorticity is mainly observed near the bed due to bottom friction. Low negative values are only observed at the leading tip. Vorticity over a wet bed depends on water height: eddy formation with positive vorticity is observed for $d \ll d_0$ due to wave breaking. Negative vorticity is also observed in this case due to the so called "mushroom" jet. The breaking process is stopped when increasing d, in such a way that negative vorticity is only observed at the interface between both fluids.

Acknowledgments

One of the writers, A. J. C. Crespo, would like to acknowledge Dr. Imre M. Janosi for kindly providing details about the experimental setup. R. A. Dalrymple acknowledges support of the Coastal Geosciences program of the Office of Naval Research.

References

Batchelor, G. K. (1974). *Introduction to fluid dynamics*, Cambridge University Press, Cambridge, U.K.

Benz, W. (1990). "Smoothed particle hydrodynamics: A review." *The numerical modelling of nonlinear stellar pulsations: Problems and prospects*, J. R. Butchler, ed., Kluwer Academic, Dordrecht, The Netherlands, 269–288.

Benz, W., and Asphaug, E. (1994). "Impact simulations with fracture. I: Methods and tests." *Icarus*, 107, 98–116.

Benz, W., and Asphaug, E. (1995). "Simulations of brittle solids using smoothed particle hydrodynamics." *Comput. Phys. Commun.*, 87, 253–265.

Bonet, J., and Kulasegaram, S. (2000). "Corrections and stabilization of smooth particle hydrodynamics methods with applications in metal forming simulations." *Int. J. Numer. Methods Eng.*, 47, 1189–1214.

Bonet, J., and Lok, T.-S. L. (1999). "Variational and momentum preservation aspects of smoothed particle hydrodynamics formulations." *Comput. Methods Appl. Mech. Eng.*, 180, 97–115.

Chanson, H., Aoki, S., and Maruyama, M. (2003). "An experimental study of tsunami runup on dry and wet horizontal coastlines." *Sci. Tsunami Hazards*, 20(5), 278–293.

Colagrossi, A., and Landrini, M. (2003). "Numerical simulation of interfacial flows by smoothed particle hydrodynamics." *J. Comput. Phys.*, 191, 448–475.

Crespo, A. J. C., Gómez-Gesteira, M., and Dalrymple, R. A. (2007a). "Boundary conditions generated by dynamic particles in SPH methods." *Comput., Mater., Continua*, 5(3) 173–184.

Crespo, A. J. C., Gómez-Gesteira, M., and Dalrymple, R. A. (2007b). "3D SPH simulation of large waves mitigation with a dike." *J. Hydraul. Res.*, 45(5), 631–642.

Dalrymple, R. A., Knio, O., Cox, D. T., Gómez-Gesteira, M., and Zou, S. (2002). "Using a Lagrangian particle method for deck overtopping." *Proc., Waves 2001*, ASCE, Reston, Va., 1082–1091.

Gingold, R. A., and Monaghan, J. J. (1977). "Smoothed particle hydrodynamics: Theory and application to non-spherical stars." *Mon. Not. R. Astron. Soc.*, 181, 375–389.

Gómez-Gesteira, M., Cerqueiro, D., Crespo, C., and Dalrymple, R. A. (2005). "Green water overtopping analyzed with a SPH model." *Ocean Eng.*, 32, 223–238.

Gómez-Gesteira, M., and Dalrymple, R. A. (2004). "Using a 3D SPH method for wave impact on a tall structure." *J. Waterway, Port, Coastal, Ocean Eng.*, 130(2), 63–69.

Henderson, F. M. (1966). *Open channel flow*, Macmillan, New York.

Janosi, I. M., Jan, D., Szabo, K. G., and Tel, T. (2004). "Turbulent drag reduction in dam-break flows." *Exp. Fluids*, 37, 219–229.

Klemp, J. B., Rotunno, R., and Skamarock, W. C. (1997). "On the propagation of internal bores." *J. Fluid Mech.*, 331, 81–106.

Leal, J. G. A. B., Ferreira, R. M. L., and Cardoso, A. H. (2006). "Dam-break wave-front celerity." *J. Hydraul. Eng.*, 132(1), 69–76.

Liu, G. R. (2003). *Mesh free methods: Moving beyond the finite element method*, CRC Press, Boca Raton, Fla., 345–368.

Lucy, L. (1977). "A numerical approach to the testing of fusion process." *Astron. J.*, 82, 1013–1024.

Monaghan, J. J. (1982). "Why particle methods work." *SIAM J. Sci. Comput. (USA)*, 3, 422–433.

Monaghan, J. J. (1989). "On the problem of penetration in particle methods." *J. Comput. Phys.*, 82, 1–15.

Monaghan, J. J. (1992). "Smoothed particle hydrodynamics." *Annu. Rev. Astron. Astrophys.*, 30, 543–574.

Monaghan, J. J. (1994). "Simulating free surface flows with SPH." *J. Comput. Phys.*, 110, 399–406.

Monaghan, J. J. (1996). "Gravity currents and solitary waves." *Physica D*, 98, 523–533.

Monaghan, J. J. (2000). "SPH without tensile instability." *J. Comput. Phys.*, 159, 290–311.

Monaghan, J. J., Cas, R. F., Kos, A., and Hallworth, M. (1999). "Gravity currents descending a ramp in a stratified tank." *J. Fluid Mech.*, 379, 39–70.

Monaghan, J. J., and Kos, A. (1999). "Solitary waves on a Cretan Beach." *J. Waterway, Port, Coastal, Ocean Eng.*, 125(3), 145–154.

Monaghan, J. J., and Kos, A. (2000). "Scott Russell's wave generator." *Phys. Fluids*, 12, 622–630.

Monaghan, J. J., and Lattanzio, J. C. (1985). "A refined method for astrophysical problems." *Astron. Astrophys.*, 149, 135–143.

Montes, J. S. (1998). *Hydraulics of open channel flow*, ASCE Press, Reston, Va., 697.

Ritter, A. (1892). "Die fortpflanzung der wasserwellen." *Z. Ver. Dtsch. Ing.*, 36(24), 947–954.

Stansby, P. K., Chegini, A., and Barnes, T. C. D. (1998). "The initial stages of dambreakflow." *J. Fluid Mech.*, 374, 407–424.

Verlet, L. (1967). "Computer experiments on classical fluids. I. Thermodynamical properties of Lennard-Jones molecules." *Phys. Rev.*, 159, 98–103.

Violeau, D., and Issa, R. (2006). "Numerical modelling of complex turbelent free-surface flows with the SPH method: an overview." *Int. J. Numer. Methods Fluids*, 53, 277–304.